Computational Design of Next Generation Atom Transfer Radical Polymerization Ligands†

Madeleine Stewart,[a] Li-Juan Yu,[a] Michael S. Sherburn[a] * and Michelle L. Coote[a] *

Benchmarked density functional theory is used to design and evaluate a series of novel atom transfer radical polymerization (ATRP) catalysts with a view to identifying those which best promote a model ATRP reaction between the $[LCu^{I}]^{+}$ catalyst and methyl α-bromoisobutyrate in acetonitrile. Calculations were performed at the ωB97XD/Def2TZVP//ωB97XD/SDD/6-31G(d) level of theory with CPCM solvent corrections. Locating the axial N of the tetradentate ATRP ligand at a sterically unhindered quinuclidine bridgehead site, with the cage carrying three pendant 2-pyridyl arms to serve as equatorial ligands causes a significant increase in activity. The effects are greater for the CH_2-linked quinuclidine cages compared with the O-linked cages, although both systems outperform the best available ATRP ligands in current use. Inclusion of this cage structure introduces opportunities for stereoisomerism, and while all stereoisomers examined function as effective catalysts, there is significant variation in performance. Incorporation of electron donating 4-(dialkylamino) groups on the 2-pyridyl arms improves ligand activity by stabilizing Cu^{II} over Cu^{I}, however, one needs to be careful of unfavorable steric crowding, particularly for some stereoisomers. Replacing the 2-pyridyl arms with other types of neutral heterocycles, such as NHC-containing heterocycles and imidazoles, does not appear to offer an advantage over pyridine. However, ligands with negatively charged donor nitrogens could offer 10 orders of magnitude improvement in catalyst activity over the best available neutral ligands, which could help make ATRP and other small molecule processes that employ ATRP catalysts applicable to unactivated alkyl halides.

INTRODUCTION

Atom Transfer Radical Polymerisation (ATRP)[1,2] is one of the leading methods for controlling radical polymerisation, permitting the production of precisely defined polymers.[3-6] Control in ATRP is achieved through the introduction of a rapid and dynamic equilibrium between a dormant alkyl halide species and a radical chain which can add to monomer, as displayed in Scheme 1. Due to the strength of the alkyl halide bond, a mediator, usually a Cu (I) complex with tri or tetradentate nitrogen-based ligands, is needed to effect and modulate this equilibrium via an inner-sphere electron transfer mechanism.[7,8]

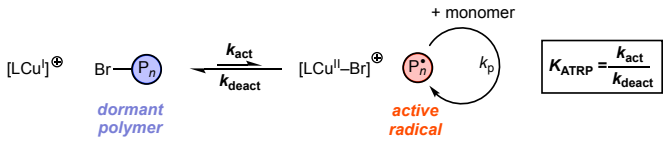

Scheme 1. Control equilibrium in Cu (I)-catalyzed ATRP.

The rational design of highly active catalysts has been and still remains a primary objective in ATRP research.[9] The most active ATRP catalysts currently available[10-12] afford values of k_{act} for common ATRP initiators that are over 8 orders of magnitude faster than the corresponding values of the originally-used[1] Cu(I)Br precatalyst – 2,2-bipyridine ligand system (Chart 1). Nonetheless, even the most active catalysts currently available are unable to cleave the strong C-Br bonds in the dormant alkyl bromide in vinyl and olefin-based polymerizations (e.g., unactivated primary alkyl bromides such as 1-bromoethyl acetate in vinyl acetate polymerization and bromoethane in ethylene polymerization). The scope of other processes, such as atom transfer radical addition[13] and *sp³* C–N cross-coupling,[14] that use ATRP catalysts to mediate C–X activation is likewise limited. Higher catalyst activity also suppresses unwanted side reactions by lowering the activator concentration at equilibrium, broadens the scope of possible alkyl halide initiators and permits lower catalyst loadings.[9]

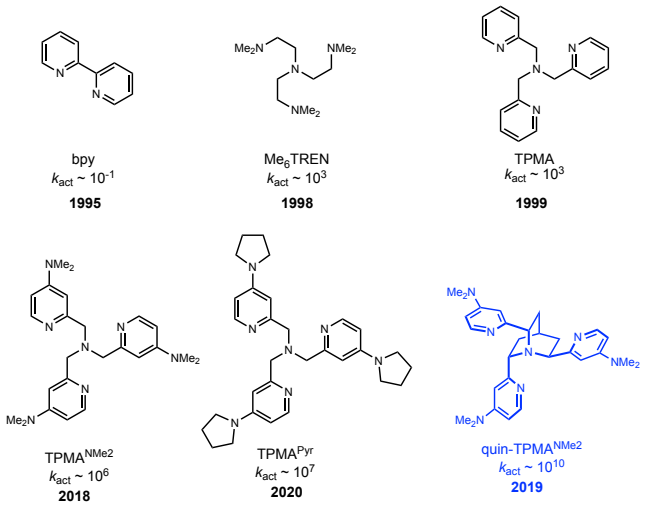

Chart 1. Key ligands that have been important in ATRP catalyst development. Activation rate constants (L mol^{-1} s^{-1}) are given for ATRP with the initiator $(CH_3)_2C(COOCH_3)Br$ in the presence of $Cu^{I}Br$ in acetonitrile at 22 °C.[18] Ligand quin-TPMA^{NMe2} (in blue) has yet to be synthesized; its computationally predicted rate coefficient is shown in lieu of an experimental value.[15]

Structure-reactivity relationships with respect to the catalyst and initiator in ATRP are reasonably well understood.[7,8,15,16] The activity of the ATRP catalyst is governed largely by the ability of the ligand to stabilise the Cu^{II} species over the Cu^{I} species.

† Electronic Supplementary Information (ESI) available: PDF File containing supple- mentary tables, total energies and geometries. See DOI: 10.1039/x0xx00000x

* [a] *Research School of Chemistry, Australian National University, Canberra, Austral ian Capital Territory 2601, Australia. Emails: michael.sherburn@anu.edu.au michelle.coote@anu.edu.au*

Naturally, ligands with a higher electron-donating capacity tend to stabilise the oxidised species more effectively, which is why, for example, the *para*-amino substituted TPMA^{NMe2} ligand is significantly more effective than TPMA itself. Because the alkyl halide activation occurs via inner-sphere electron transfer, [7,8,17] the reaction site needs to be available, without being too sterically encumbered by the ligand. Thus, for example, Me_6TREN is significantly more effective than Et_6TREN.[18] Additionally, the energy barrier will be smaller if the ligand conformational changes throughout the process are minimised.

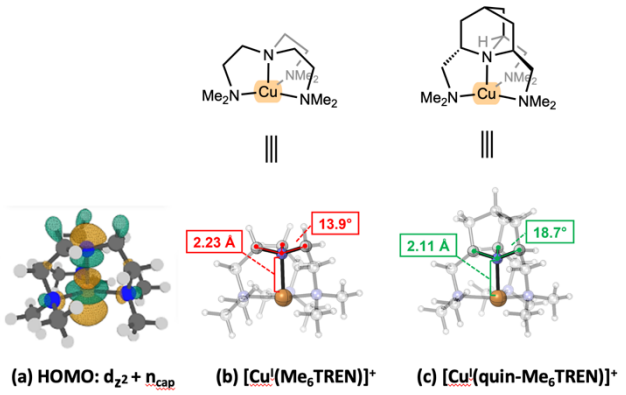

Figure 1. (a) HOMO and (b) geometry and POAV *N*-pyramidalization angles for [Cu^{I}(Me$_6$TREN)]$^+$ and also (c) an analogue in which the axial nitrogen is enclosed in a quinuclidine cage. Images taken with permission from Ref 15.

Recently, based on computational studies, we proposed a new strategy for further increasing catalyst activity, beyond current experimental limits.[15] For nitrogen-based ligands at least, we showed that the oxidation potential of the [LCu^{I}]$^+$ species follows Koopman's theorem: that is, it is inversely proportional to the energy of the highest occupied molecular orbital (HOMO) of the complex. Because this HOMO also contains a node along the axial Cu-N bond, we predict that, all things being equal, decreases to the axial Cu-N bond length should be accompanied by destabilization of the HOMO and hence, by Koopman's theorem, the promotion of oxidation. Thus, we leveraged the sterically unhindered yet electron rich nature of the bridgehead amine nitrogen of quinuclidine systems to promote shorter axial Cu–N bond lengths (see Figure 1). Based on benchmarked density functional theory calculations, we predicted that when used as a ligand, the quinuclidine derivative of Me_6TREN has a k_{act} value for the ATRP reaction with $(CH_3)_2C(COOCH_3)Br$ rate that is 350 times faster than that of Me_6TREN.[15] Likewise, the quinuclidine derivative of TPMA^{NMe2} is predicted to be approximately 4 orders of magnitude more active than TPMA^{NMe2} itself, which would make it 3 orders magnitude more active than any synthesised catalyst to date (see Chart 1).[15]

While there is synthetic precedent in the patent literature for analogues of the tripodal quinuclidine ligands carrying 2-(naphthalen-1-yl)pyridyl and 2-(6-bromo)pyridyl arms,[19] quin-TPMA^{NMe2} is yet to be synthesised, with the substituted quinuclidine cap proving synthetically challenging. The corresponding triphenyl-substituted quinuclidine was synthesised in 8 steps from 4-pyridone by Corey in 2010,[20] and the presence of the three pyridyl groups in place of the phenyls was anticipated to lead to significant additional synthetic challenges and complications. We envisaged a solution to this problem that involved a diverted total synthesis strategy,[21] whereupon we would replace one of the methylene groups in the quinuclidine cap with an oxygen. Synthetically, this would in principle permit a simpler synthesis, as seen in the proposed synthetic route outlined in Scheme 2. Thus, a twofold aza-Michael addition of ammonia to a simple Claisen-Schmidt condensation product would be expected to give a 2,6-disubstituted 4-piperidone,[22] which could be reduced to the secondary alcohol then converted into the caged hemiaminal ether **L1** using the condensation conditions of Hardgetter and Ott.[23] However, this raises the questions to what extent does the oxygen alter the activity of the ligand, and which if any of the possible diastereomeric products **L1**-**L4** (which differ in relative configurations at C2, C4 and C6) is most effective as a ligand. Moreover, for both the O and CH_2 linked quinuclidine systems, to what extent can the activity be further tuned by altering the *para*-substituent of the pyridine and/or replacing the pyridine altogether with other heterocycles?

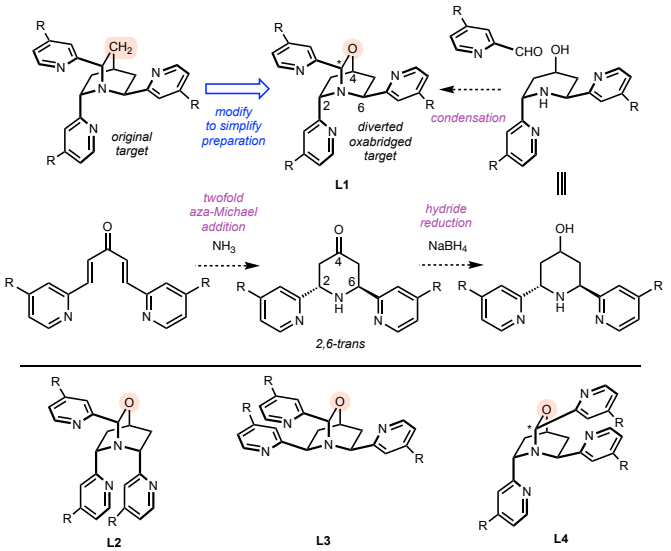

Scheme 2. The proposed synthesis of analogues of Quin-TPMA^{NMe2}. The production of four different diastereomers (**L1**, **L2**, **L3** and **L4**) is possible with an oxygen in the quinuclidine cap. When the oxygen is replaced with a CH_2 linker, **L2**, **L3** and **L4** are equivalent.

To address these questions, and thereby identify the most promising ATRP ligands for follow-up synthetic studies, in the present work we used accurate computational chemistry to study the kinetics and thermodynamics of the ATRP reaction of methyl α-bromoisobutyrate,[7,8,15,16] chosen for consistent comparison with previous studies, for a broad range of ligands (Chart 2). Included in this ligand library are molecules with different *para* substituents and different heterocycles to elucidate the effect of each of these components. Each ligand was studied with both an oxygen and a CH_2 in the quinuclidine core, and the ligands with different *para* substituents were studied for the three most synthetically accessible diastereomers (**L1**, **L2** and **L3**) to determine the impact of these factors on mediator

activity in order to better inform the synthesis of more active ligands. Ligand **L4** was not included in this study since its generation in the synthetic pathway shown in Scheme 2 was considered unlikely. In principle, both **L1** and **L4** can be formed in the final condensation step of Scheme 2. However, since **L4** is the more sterically strained hence less thermodynamically stable (i.e. non-propeller) C* epimer of **L1**, its formation is disfavoured.

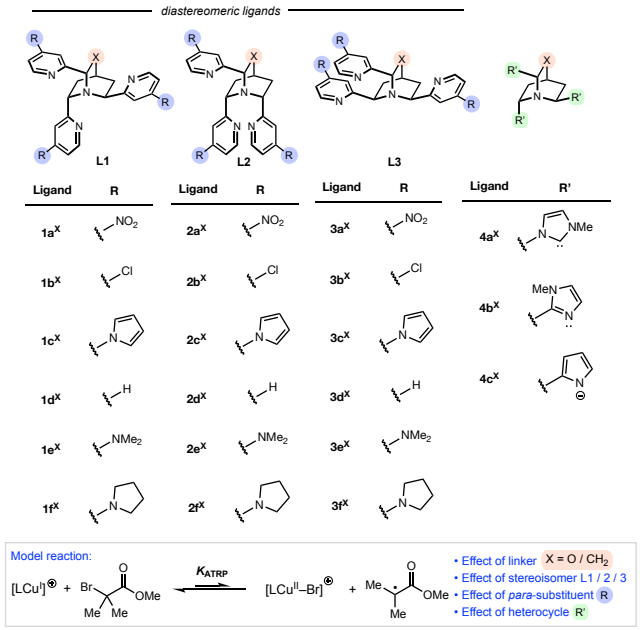

Chart 2. Scope of the present work. Note that only two diastereomers exist for X = CH_2, meaning that $2a^{CH2}$ is equivalent to $3a^{CH2}$, $2b^{CH2}$ is equivalent to $3b^{CH2}$, etc.

Computational Procedures

Standard density functional theory (DFT) calculations were performed using Gaussian 16[24] at a level of theory previously shown to reproduce experimental k_{act} values of ATRP reactions.[7] Geometries and frequencies were first calculated in the gas phase using ωB97XD,[25] with a mixed basis set of SDD[26] for Cu and 6-31G(d) for other atoms.[27] Single point energies were then calculated using ωB97XD/Def2TZVP in acetonitrile using the CPCM solvation model.[28] Gibbs free energies in acetonitrile solution were then calculated via a thermocycle method, in conjunction with the harmonic oscillator - rigid rotor approximation, and include a correction for the change of state from 1atm to 1M.[29] Total energies and optimized geometries, including heat maps of the Cu-ligand bond lengths in the $[LCu^{I}]^{+}$, $[LCu^{II}]^{2+}$ and $[LCu^{II}Br]^{+}$ complexes, are provided in the Electronic Supplementary Information.

Results and Discussion

Figure 2a shows the predicted reaction Gibbs free energies (298 K, acetonitrile) for the model ATRP reaction of methyl α-bromoisobutyrate with the full test set of catalysts in Chart 2; corresponding forward and reverse barrier heights for a subset of the ligands are provided in Figure 3. To better understand the trends in Figure 2a, we used a simple Hess cycle (Scheme 3) to express the reaction Gibbs free energy as the sum of the reaction Gibbs free energy for the (hypothetical) dissociative electron transfer reaction between the catalyst and substrate (ET), and that of the halogen association reaction between the oxidised catalyst and the bromide ion (HA). The resulting ET and HA contributions are provided in Figure 2b. It should be noted that Scheme 3 is a Hess cycle; the reaction itself occurs via a single step inner-sphere electron transfer mechanism so that the large energetic cost of oxidising the catalyst is simultaneously offset by the energy gained by halogen association.

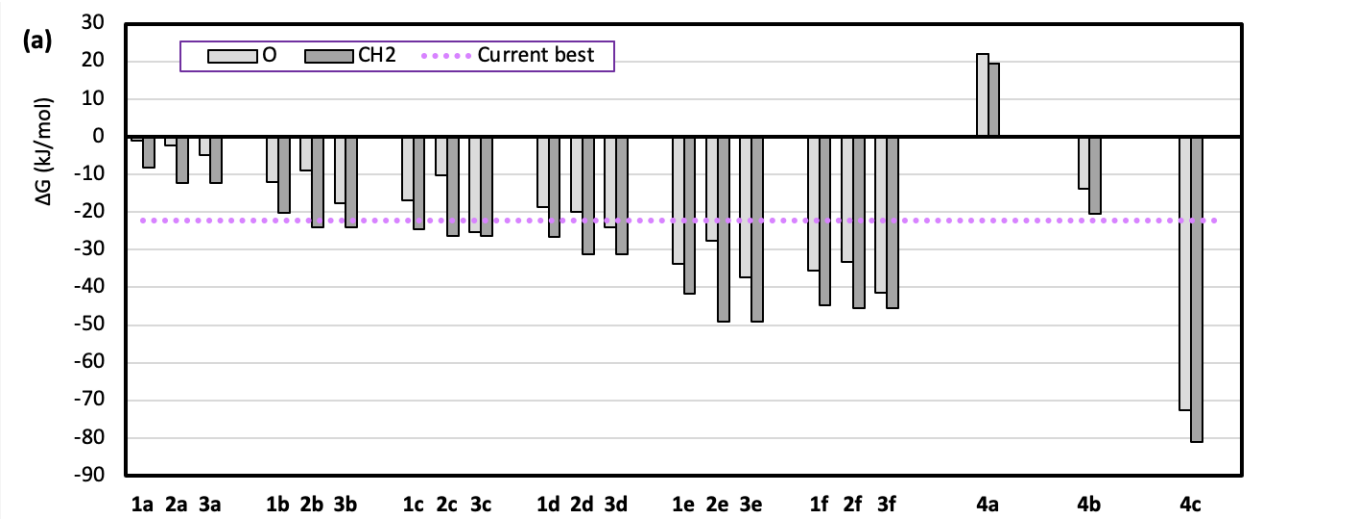

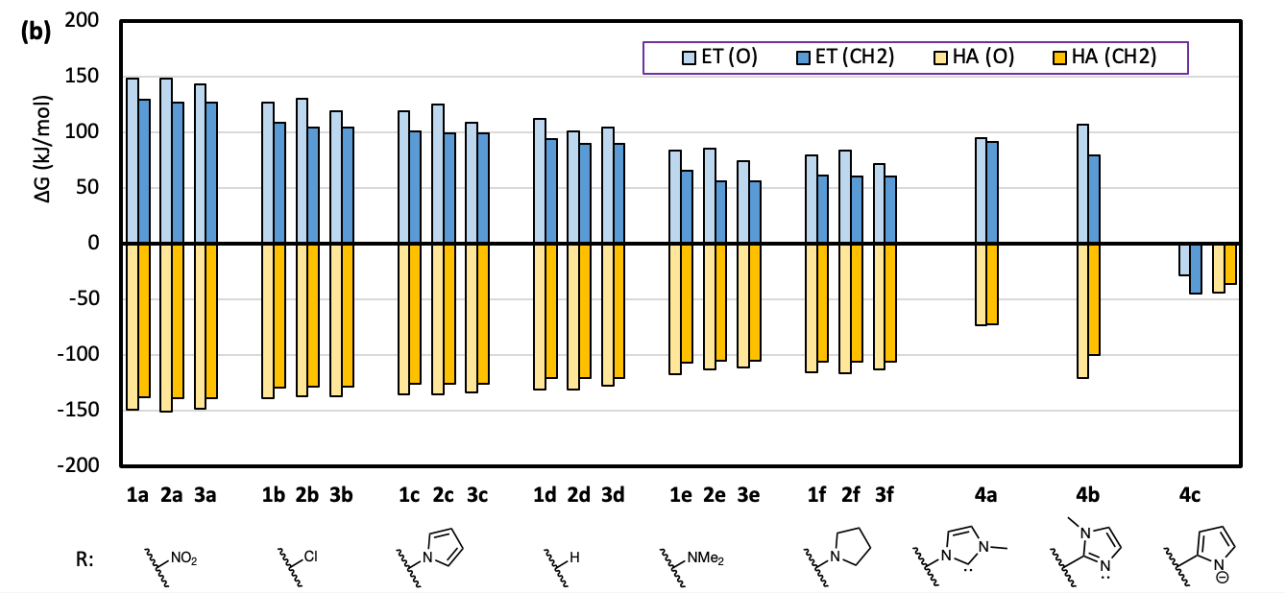

Figure 2. (a) Reaction Gibbs free energy (ΔG, kJ mol^{-1}, 298 K, acetonitrile) for the model ATRP reaction of methyl α-bromoisobutyrate with the full test set of catalysts in Chart 2. The corresponding experimental value for the synthesised ligand having the best reported thermodynamics to date (TPMA^{NMe2}) is given for comparison.[12] (b) Electron transfer (ET) and halogen affinity (HA) contributions (see Scheme 3 for definitions) to the overall reaction Gibbs free energy under the same conditions.

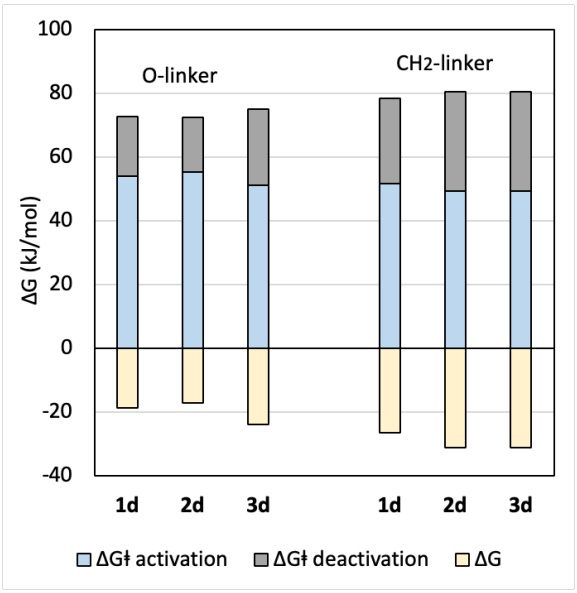

Figure 3. Forward (activation) and reverse (deactivation) Gibbs free energy barriers and reaction energies (ΔG‡, kJ mol^{-1}, 298 K, acetonitrile) for the model ATRP reaction of methyl α-bromoisobutyrate with both the O-linked and CH_2-linked **1d**, **2d** and **3d** ligands in Chart 2.

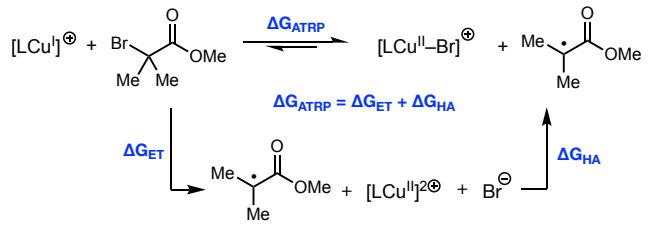

Scheme 3. Hess cycle showing the relationship between the reaction Gibbs free energy for the ATRP reaction, and that for the dissociative electron transfer between the reactants (ET) and association of the resulting bromide with the oxidised catalyst (HA).

Effect of Linker Atom.

The principal objective of the present work was to assess whether the oxygen linker had a detrimental effect on catalyst performance. From Figure 2a, it is clear that the oxygen-linked species follow the same trends as their CH_2 linked analogues, but their reactions are generally less thermodynamically favourable than their corresponding CH_2 linked counterparts by 5-10 kJ mol^{-1}. Nonetheless, even with the O-linker, the *para*-amino substituted ligands (i.e., **1e**/**2e**/**3e** and **1f**/**2f**/**3f**) display considerably more exergonic reactions than the best-available ligands, TPMA^{NMe2} and TPMA^{Pyr}. Moreover, if we examine the barrier heights for the unsubstituted systems (Figure 3), we see that while their trends follow those of the thermodynamics, the difference in barrier heights for the forward (activation) reaction between corresponding O-linked and CH_2-linked catalysts are much smaller than the differences in their thermochemistry. As a result, the O-linked catalysts strike the best compromise between having low activation and deactivation barriers, thus making them particularly attractive as control agents. In summary, the presence of the quinuclidine cage significantly improves catalyst performance over the corresponding ligands that lack this cage structure, and even the O-linked systems would be worth pursuing synthetically.

From Figure 2b, it is seen that the O-linked species are harder to oxidise than their corresponding CH_2-linked counterparts, presumably due to the σ-inductive effects of the oxygen linker which renders the binding nitrogens less electron rich and less able to stabilize Cu^{II} over Cu^{I}. For the same reason, the halogen association energies for the O-linked species are systematically more exergonic than their CH_2-linked counterparts. Overall, the O-linked species are less effective than their CH_2-linked counterparts because their more favourable HA values only partially offsets their less favourable ET values. To help understand why,

the structures of the Cu(I) complexes of the quin-TPMA-substituted compounds (i.e., **1d**/**2d**/**3d**) were examined. Figure 4 shows the axial and average equatorial Cu-N bond lengths of the respective $[LCu^{I}]^{+}$ and $[LCu^{II}Br]^{+}$ complexes; individual bond lengths are provided in Tables S1 and S3 of the Electronic Supplementary Information. While axial Cu–N distances are similar between corresponding O-linked and CH_2-linked ligands, the equatorial bonds are longer because the shorter O-C versus C-C bond in the quinuclidine cages effectively makes the arms of the tripodal ligands shorter and it becomes harder to optimally accommodate all 4 Cu-N bonds simultaneously. However, these longer Cu-N bonds in the O-linked catalysts provide more room around the Cu centre, which is presumably why the O-linked compounds are more reactive than one would expect based on the reaction energies.

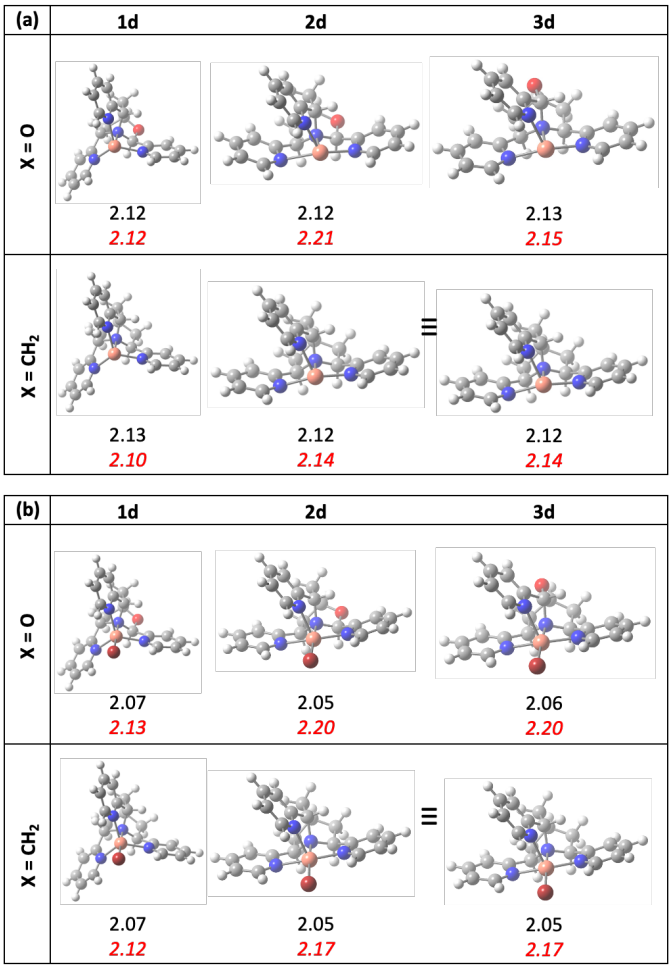

Figure 4. (a) Binding of **1d**, **2d** and **3d** to Cu(I). The axial (black) and average equatorial (red italic) Cu-N bond lengths (Å) are also shown. Individual bond lengths are shown in Table S1 of the Supporting Information. (b) Corresponding Cu(II) complexes of **1d**, **2d** and **3d**. Individual bond lengths are shown in Table S3 of the Supporting Information.

Stereochemistry.

The stereochemistry of the ligand has a significant effect on the thermodynamics of the ATRP reaction (Figure 2). For the CH_2-linked species, the (equivalent) **L2**/**L3** isomers generally give rise to more exothermic reactions than the **L1** isomers. For the O-linked species the **L3** ligand also outperforms **L1**. However, **L2**, which in the O-linked series is not equivalent to **L3**, tends to give the least exothermic reactions. The **L1** isomer displays the best geometry for binding Cu^{I}, giving rise to the shortest average Cu-N distances, both in the parent quin-TPMA systems (Figure 4) and the *para*-substituted ligands (Figure 5). This is because the propeller geometry of the **L1** isomer is best able to accommodate all 4 Cu-N bonds in the preferred tetrahedral geometry of the Cu^{I} complexes. Complexes of Cu^{I} with **L2** and **L3** are distorted from the tetrahedral form, and are best approximated as trigonal bipyramidal (see for example Figure 4a). Despite this, the **L3** ligand is still able to accommodate all 4 Cu-N bonds with only minor distortions compared with **L1**, except in the two bulkiest cases (**3c**^{CH2} and **3f**^{CH2}). Importantly, upon oxidation the trigonal bipyramidal Cu^{II} complexes can better accommodate the **L3** versus **L1** isomers (Figure 4b), and this gives the **L3** isomers the advantage. However, in O-linked compounds, the **L2** isomer is not able to bind effectively, with at least one Cu-N bond semi-detaching (i.e., Cu–N > 3Å) in all but the least hindered *para*-unsubstituted ligand (i.e. **2d**^{O}). These problems, which stem from the C-O linker bond effectively making one of the tripodal arms shorter, remain in the oxidised form (Figure 5b) and result in this isomer being least effective.

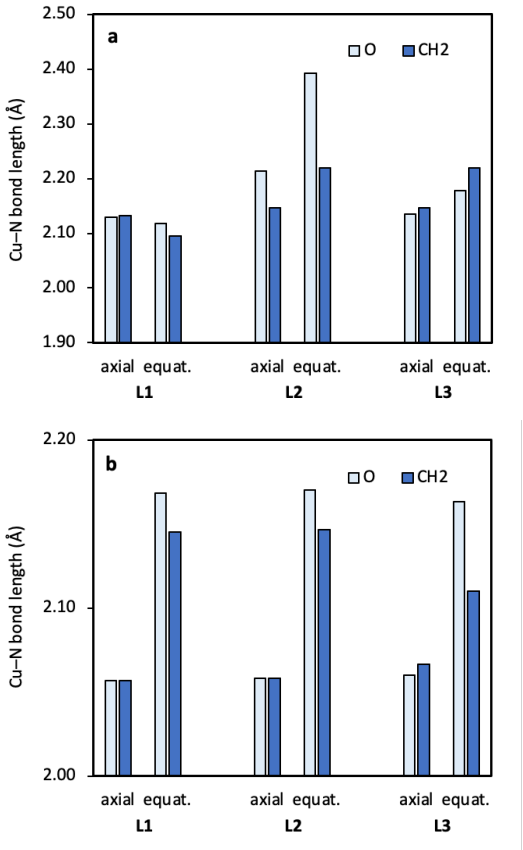

Figure 5. (a) Average axial and equatorial bond lengths (Å) for the Cu^{I} complexes of the *para*-TMPA substituted quinuclidine ligands in Chart 1 (i.e. all except **4a**/**4b**/**4c**), with averages calculated separately for the **L1**, **L2** and **L3** stereoisomers and O-linked and CH_2-linked compounds. Individual bond lengths are shown in Table S1 of the Supporting

Information. (b) Corresponding data for the $[LCu^{II}Br]^+$ complexes of the ligands. Individual bond lengths are shown in Table S3 of the Supporting Information.

***Para* Substituents.**

As expected, the ATRP equilibrium is significantly affected by substituents *para* to the donor nitrogen on the 2-pyridyl moiety, with electron withdrawing groups such as NO_2 promoting the reaction to a much lesser extent than electron donors such as NMe_2 and *N*-pyrrolidinyl. This effect has previously been observed; the activity of the original ATRP ligand, 2,2'-bipyridine was found to increase with the inclusion of *para* electron donating groups and decrease with the inclusion of *para* electron withdrawing groups.[30] Indeed, this observation was leveraged to design the most active synthesised ligands to date, by substituting TPMA with *para*-NMe_2 and *para*-*N*-pyrrolidinyl groups.[10-12] Consistent with previous studies,[7,15] electron donation reduces the energy cost for ET by helping to stabilize Cu^{II} relative to Cu^{I}, but in doing so also makes HA less exergonic by reducing the electrostatic interaction between Cu^{II} and the Br^- (see Figure 2b). Nonetheless, the former effect outweighs the latter leading to increased performance with incorporation of electron donors as *para*-substituents.

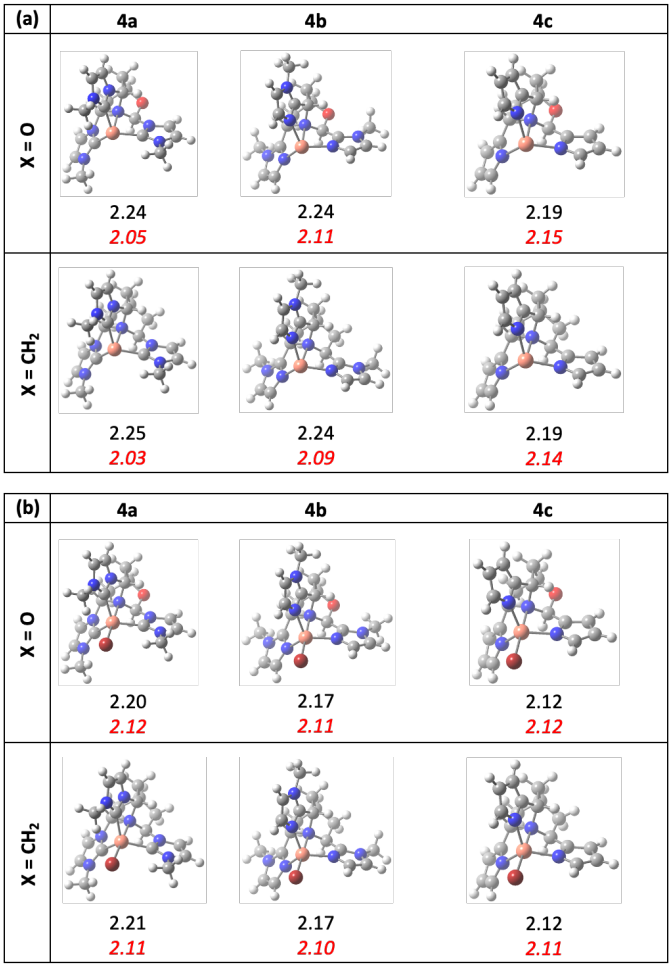

Figure 6. (a) Binding of **4a**, **4b** and **4c** to Cu(I). The axial (black) and average equatorial (red italic) Cu-N bond lengths (Å) are also shown. (b) Corresponding Cu(II) complexes of **4a**, **4b** and **4c**.

While the effects of *para*-substituents are largely as anticipated, it is worth noting that bulky *para*-substituents display less exergonic behaviour than otherwise expected, particularly in the more crowded **L2** and **L3** isomers. Thus, for example, as the strongest donor, the *para*-*N*-pyrrolidinyl substituted ligand is expected to display the best overall thermodynamics. Indeed, it does out-perform *para*-NMe_2 for the **L1** ligand but loses some or all of its advantage in the **L2**/**L3** ligands. As a result, the L3 *para*-NMe_2 ligand (**3e^{CH2}**) is predicted to perform best overall with CH_2-linker, though with the O-linker the **L3** *para*-*N*-pyrrolidine ligand (**3f^{O}**) narrowly retains its advantage over **3e^{O}**.

Alternative heterocycles.

Finally, we screened three additional heterocycles, as alternatives to the 2-pyridyl substituents on our quinuclidine ligands. Of these, the *N*-heterocyclic carbene (NHC) ligand (**4a**) gave rise to endergonic ATRP reactions, the *N*-methylimidazol-2-yl ligand (**4b**) gave rise to slightly less exergonic reactions than those with the corresponding 2-pyridyl ligands, while the negatively charged (i.e. *N*-deprotonated) 2-pyrrolyl ligand gave rise to significantly more exergonic reactions than any other ligand known or tested (**4c**). In both cases the O-linked species was again slightly less active than the CH_2-linked species, but these differences were minor when compared with the differences arising from alternative heterocycles.

The poor performance of the NHC ligand was initially surprising as it was expected to be a good electron donor. However, on examination of Figure 2b it was clear that the problem was not its ability to stabilize Cu^{II} over Cu^{I}. In fact, its ET term is very similar to that of 2-pyridyl; however, its halogen association is much less exergonic than any other as increased steric crowding lengthens the Cu-Br bond (Cu-Br bond lengths are 2.41 Å in **4a^{CH2}** and 2.34 Å **1d^{CH2}**, respectively). The *N*-methylimidazol-2-yl ligand displays behaviour that is more analogous the 2-pyridyl ligands, though performs slightly worse than anticipated because the more hindered heterocycle leads to an increase in the axial Cu-N bond (Figure 6). Unsurprisingly, the negatively charged ligand stabilizes Cu^{II} over Cu^{I} so much so that even the electron transfer term is exergonic. For the test reaction, this process is clearly too favourable for an effective ATRP as the deactivation reaction would be inhibited and there would be no control. However, such ligands would potentially be suitable for unactivated alkyl halides, depending on activation and deactivation kinetics.

CONCLUSIONS

Motivated by a possible synthetic pathway towards oxygen analogues of the highly active but synthetically challenging quin-$TPMA^{NMe2}$ ligand, a computational study was undertaken to screen a series of potential ATRP catalysts to better understand structure-reactivity trends and identify promising synthetic targets (Figure 7). "Tying back" the three alkyl substituents of the axial N of the ATRP ligand in a quinuclidine ring then substituting each with equatorial donor groups leads to tetradentate ligands with significantly increased activity. The effects are greater for

(CH_2-linked) quinuclidine cages compared with their hemiaminal ether (O-linked) analogues. Nonetheless, the latter are still predicted to out-perform the best available ATRP ligands in current use.

The adoption of this new ligand design introduces opportunities for stereoisomerism, and while all stereoisomers examined bind Cu^{I} and Cu^{II} and function as effective catalysts, there is significant variation in performance. Interestingly, the most effective isomers (generally **L3** in Scheme 2) are not those best able to bind Cu^{I} in its preferred tetrahedral geometry, rather those that bind in a less optimal trigonal bipyramidal geometry and thus undergo smaller changes upon oxidation. As with the non-caged ligands, inclusion of electron donating *para*-amino groups on the pyridine arms improves ligand activity by stabilizing Cu^{II} over Cu^{I}, however one needs to be additionally careful of unfavourable steric crowding, particularly for **L2** and **L3** diastereomers. While not examined here, an additional attractive feature of this caged ligand system is its chirality, which offers thus far unexplored opportunities for enantioselective catalysis.

Finally, replacing the pyridine arms with other types of neutral heterocycles, such as NHCs and imidazoles, does not appear to offer an advantage over pyridine. However, if synthetically attainable, ligands with negatively charged donor nitrogens could offer 10 orders of magnitude improvement in catalyst activity over the best available neutral ligands, which could help make ATRP and other small molecule processes that employ ATRP catalysts applicable to unactivated alkyl halides. Work to synthesise and test the most promising, synthetically accessible ligands identified through this study is currently underway.

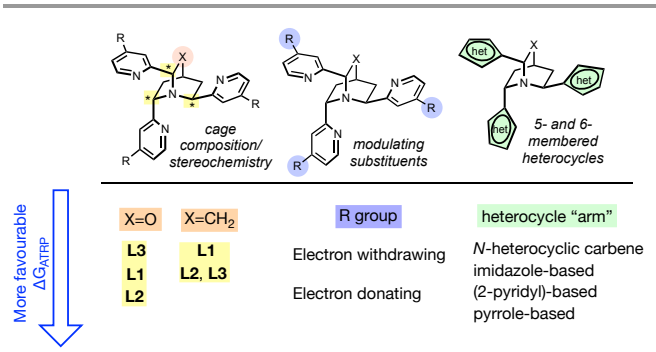

Figure 7. The effect of different aspects of quin-TPMAN^{Me2} based ligands on the thermodynamics of ATRP.

Author Contributions

All authors contributed to the manuscript.

Conflicts of interest

There are no conflicts to declare.

Acknowledgements

The authors acknowledge an ARC Laureate Fellowship to M.L.C. (FL170100041), ARC Discovery funding to M.S.S. (DP160104322) and generous supercomputing time from the National Computational Infrastructure, and thank Professor Tony Hill for useful discussions

Notes and references

1. J. S. Wang and K. Matyjaszewski, *J. Am. Chem. Soc.*, 1995, **117**, 5614–5615.
2. M. Kato, M. Kamigaito, M. Sawamoto and T. Higashimura, *Macromolecules*, 1995, **28**, 1721-1723.
3. K. Matyjaszewski, *Adv. Mater.*, 2018, **30**, 1706441.
4. K. Matyjaszewski, *Macromolecules*, 2012, **45**, 4015-4039.
5. M. Ouchi, T. Terashima and M. Sawamoto, *Acc. Chem. Res.*, 2008, **41**, 1120-1132.
6. K. Parkatzidis, H. S. Wang, N. P. Truong and A. Anastasaki, *Chem*, 2020, **6**, 1575-1588.
7. C. Fang, M. Fantin, X. C. Pan, K. de Fiebre, M. L. Coote, K. Matyjaszewski and P. Liu, *J. Am. Chem. Soc.*, 2019, **141**, 7486-7497.
8. C. Y. Lin, M. L. Coote, A. Gennaro and K. Matyjaszewski, *J. Am. Chem. Soc.*, 2008, **130**, 12762-12774.
9. F. Lorandi and K. Matyjaszewski, *Isr. J. Chem.*, 2020, **60**, 108-123.
10. A. E. Enciso, F. Lorandi, A. Mehmood, M. Fantin, G. Szczepaniak, B. G. Janesko and K. Matyjaszewski, *Angew. Chem. Int. Ed.*, 2020, **59**, 14910-14920.
11. T. G. Ribelli, F. Lorandi, M. Fantin and K. Matyjaszewski, *Macromol. Rapid Commun.*, 2019, **40**.
12. T. G. Ribelli, M. Fantin, J. C. Daran, K. F. Augustine, R. Poli and K. Matyjaszewski, *J. Am. Chem. Soc.*, 2018, **140**, 1525-1534.
13. T. Pintauer and K. Matyjaszewski, *Chem. Soc. Rev.*, 2008, **37**, 1087-1097.
14. A. K. K. Fung, L. J. Yu, M. S. Sherburn and M. L. Coote, *J. Org. Chem.*, 2021, **86**, 9723-9732.
15. V. Doan, B. B. Noble, A. K. K. Fung and M. L. Coote, *J. Org. Chem.*, 2019, **84**, 15624-15632.
16. W. Tang, Y. Kwak, W. Braunecker, N. V. Tsarevsky, M. L. Coote and K. Matyjaszewski, *J. Am. Chem. Soc.*, 2008, **130**, 10702-10713.
17. A. A. Isse, A. Gennaro, C. Y. Lin, J. L. Hodgson, M. L. Coote and T. Guliashvili, *J. Am. Chem. Soc.*, 2011, **133**, 6254-6264.
18. A. K. K. Fung and M. L. Coote, *Polym. Int.*, 2021, **70**, 918-926.
19. 2004.
20. X. Gao, R. P. Singh and E. J. Corey, *Org Lett*, 2010, **12**, 1812-1814.
21. R. M. Wilson and S. J. Danishefsky, *J. Org. Chem.*, 2006, **71**, 8329-8351.
22. N. L. Magann, M. T. Blyth and M. S. Sherburn, *Angew. Chem. Int. Ed.*, 2021, **60**, 18561-18565.
23. E. Hardegger and H. Ott, *Helv. Chim. Act.*, 1953, **36**, 1186-1189.

24. M. J. Frisch, G. W. Trucks, H. B. Schlegel, G. E. Scuseria, M. A. Robb, J. R. Cheeseman, G. Scalmani, V. Barone, G. A. Petersson, H. Nakatsuji, X. Li, M. Caricato, A. V. Marenich, J. Bloino, B. G. Janesko, R. Gomperts, B. Mennucci, H. P. Hratchian, J. V. Ortiz, A. F. Izmaylov, J. L. Sonnenberg, Williams, F. Ding, F. Lipparini, F. Egidi, J. Goings, B. Peng, A. Petrone, T. Henderson, D. Ranasinghe, V. G. Zakrzewski, J. Gao, N. Rega, G. Zheng, W. Liang, M. Hada, M. Ehara, K. Toyota, R. Fukuda, J. Hasegawa, M. Ishida, T. Nakajima, Y. Honda, O. Kitao, H. Nakai, T. Vreven, K. Throssell, J. A. Montgomery Jr., J. E. Peralta, F. Ogliaro, M. J. Bearpark, J. J. Heyd, E. N. Brothers, K. N. Kudin, V. N. Staroverov, T. A. Keith, R. Kobayashi, J. Normand, K. Raghavachari, A. P. Rendell, J. C. Burant, S. S. Iyengar, J. Tomasi, M. Cossi, J. M. Millam, M. Klene, C. Adamo, R. Cammi, J. W. Ochterski, R. L. Martin, K. Morokuma, O. Farkas, J. B. Foresman and D. J. Fox, Gaussian 16 Rev. A.03, Wallingford, CT, 2016.

25. J.-D. Chai and M. Head-Gordon, *Phys. Chem. Chem. Phys.*, 2008, **10**, 6615-6620.

26. M. Dolg, U. Wedig, H. Stoll and H. Preuss, *J. Chem. Phys.*, 1987, **86**, 866-872.

27. V. A. Rassolov, M. A. Ratner, J. A. Pople, P. C. Redfern and L. A. Curtiss, *J. Comput. Chem.*, 2001, **22**, 976-984.

28. V. Barone and M. Cossi, *J. Phys. Chem. A*, 1998, **102**, 1995-2001.

29. J. M. Ho, A. Klamt and M. L. Coote, *J. Phys. Chem. A*, 2010, **114**, 13442-13444.

30. A. J. D. Magenau, Y. Kwak, K. Schröder and K. Matyjaszewski, *ACS Macro Lett.*, 2012, **1**, 508-512.